A&A 371, 997–1011 (2001)
DOI: 10.1051/0004-6361:20010459

Astronomy & Astrophysics

An active binary XY UMa revisited⋆

T. Pribulla[1], D. Chochol[1], P. A. Heckert[2], L. Errico[3], A. A. Vittone[3], Š. Parimucha[1], and M. Teodorani[3]

[1] Astronomical Institute of the Slovak Academy of Sciences, 059 60 Tatranská Lomnica, Slovakia
[2] Department of Chem. & Physics, Western Carolina University, Cullowhee, NC 28723, USA
[3] Osservatorio Astronomico di Capodimonte, Via Moiariello 16, 80131, Napoli, Italy

Received 18 December 2000 / Accepted 15 March 2001

Abstract. New extensive multicolour photoelectric photometry, performed since 1994, is presented. 17 more-or-less complete light curves were obtained and analyzed. The Wilson-Devinney code applied to the $BVRI$ light curves without the maculation effect together with published spectroscopic mass ratio and semi-major axis yielded new absolute parameters of the eclipsing pair: $m_1 = 1.10\ M_\odot$, $m_2 = 0.66\ M_\odot$, $R_1 = 1.16\ R_\odot$, $R_2 = 0.63\ R_\odot$, $a = 3.107\ R_\odot$ and the orbital inclination $i = 80.9°$. The observed orbital period changes are conclusively explained by the mutual action of the third body in the system ($P_3 = 30$ years) and the maculation effects. Simultaneous analysis of the period changes and the visual brightness excludes the possibility of their explanation by Applegate's mechanism. The differences in the maxima heights caused by the maculation exhibit variations with the period of 709 ± 10 days. The distance to the system $d = 86 \pm 5$ pc determined from the absolute dimensions and luminosities of the components is larger than the Hipparcos astrometric value $d = 66 \pm 6$ pc.

Key words. stars: binaries eclipsing – stars: individual: XY UMa – stars: pre-main sequence – stars: magnetic fields

1. Introduction

XY UMa (HD 27143, BD +55°1317) is the most active member with the shortest orbital period (P = 0.47899 days) among all RS CVn-like binaries. According to catalog of chromospherically active binary stars (Strassmeier et al. 1993), the spectral types of the components are G3V and K4-5V (see also Geyer 1980).

The system was discovered by Geyer et al. (1955) who performed extensive photometric and spectroscopic observations (Geyer 1980; Geyer & Hoffmann 1981; Geyer & Metz 1977). Their results can be summarized as follows: (i) the light curve (LC) of the system is highly variable and asymmetric, (ii) this variability is explained by the presence of dark spots with the spot activity cycle of the primary component being 3.5–4 years, (iii) the period changes are apparent and caused by the LC disturbances, (iv) overall brightness of the system changes in a sinusoidal manner with the period of about 25 years, (v) LC depressions correlate with the enhanced ultraviolet Mg II H and K emission and increased (reddening) of the $(B - V)$ index, (vi) there is no phase-dependent polarization indicating an absence of the circumbinary matter.

Arévalo & Lázaro (1990) proposed a gas stream between the components as an alternative interpretation of the LC variations in the K passband before and after the secondary minimum.

The pronounced activity of the system is displayed by high-amplitude LC variations and flare-like episodes in the visual region (Zeilik et al. 1983; Lee 1993) and is usually ascribed to the primary component. On the other hand, Lázaro & Arévalo (1996) found an extra H_α emission connected with both components. The light contribution of the secondary component is about 6–7%, hence its spot activity has only a negligible effect on the visual LC.

The brightness of XY UMa exhibits variations on different time scales: (1) night-to-night variations; (2) changes from the symmetrical to asymmetrical LC shape over about two years; (3) long-term change of the total brightness and colour over decades. The presence of the LC disturbances causes unreliable determination of the "clean" photometric parameters by several methods. Unlike other active systems (e.g., VW Cep, Baluta et al. 1991) there are virtually no intervals with immaculate LC. Detailed modeling of the spot distribution was performed either by LC modeling (Zeilik et al. 1990) or eclipse mapping (Collier Cameron & Hilditch 1997). However, this did not explain the overall acitivity of the system.

The (O–C) diagram exhibits both erratic period changes due to the LC asymmetries and long-term

Send offprint requests to: T. Pribulla,
e-mail: priblulla@ta3.sk

⋆ Tables 4 and 8 are only available in electronic form at http://www.edpsciences.org

period changes interpreted either by the light-time effect (LITE) caused by an another body in the system (Chochol et al. 1998, hereafter C&P) or Applegate's mechanism (e.g., Erdem & Güdür 1998). However, the latter possibility was not tested observationally. The presence of the third body is supported by an infrared excess of the system (Arévalo et al. 1994) and possible eclipse of the binary by a protostellar object observed in 1978–1979 (C&P). Pojmanski & Geyer (1990, hereafter P&G) attempted to separate the LC disturbances from the LITE. They proposed either a 25 or 40 year orbital period of the third body to get a good correlation between the LC asymmetry and the (O–C) residuals from the LITE fit. On the other hand, Kjurkchieva et al. (2000) supposed the constant orbital period and explained the observed period variations only by LC asymmetries.

Bedford et al. (1990) analyzed the *EXOSAT* observations and found a clear primary eclipse in the spectral range 0.05–2 keV indicating a low-extent corona with a height less than 0.75 $R_\odot$. On the other hand, *ROSAT* observation do not show any X-ray eclipses (Jeffries 1998). The observations of XY UMa in the radio region are complicated by the strong radio source in the angular distance 2.5′ from XY UMa (Geyer 1977).

The first spectroscopic elements of the primary component were determined by Rainger et al. (1991) using the CCF method. An orbital solution provided $K_1 = 119.5 \pm 2.0$ km s^{-1} and $V_0 = -9.2 \pm 1.5$ km s^{-1}. Pojmanski & Udalski (1997) were the first to determine the semi-amplitude of the *RV*s of the secondary component $K_2 = 203 \pm 16$ km s^{-1}, superimposing 30 properly shifted spectra in the red region. Pojmanski (1998) analyzed near infrared spectra using the CCF mapping technique and determined $K_1 = 122.5 \pm 1.0$ km s^{-1}, $K_2 = 202 \pm 6$ km s^{-1} and $V_0 = -10.5 \pm 1.0$ km s^{-1}. He derived the system parameters: $q = 0.61 \pm 0.05$, $m_1 \sin^3 i = 1.06 \pm 0.07\ M_\odot$, $m_2 \sin^3 i = 0.64 \pm 0.03\ M_\odot$, which we have adopted in our paper for the LCs analysis.

Kjurkchieva et al. (2000) determined *RV*s of the primary component by the polynomial fitting of the H_α profile on 21 spectra providing $K_1 = 120.7 \pm 2.9$ km s^{-1} and $V_0 = -26 \pm 3.9$ km s^{-1}. The discrepancy in V_0 in comparison with previous authors is probably an instrumental effect.

XY UMa was the target of the Hipparcos astrometric mission. The distance $d = 66 \pm 6$ pc was derived assuming the binary nature of the system. The main goals of the present paper are to further test the possible mechanisms responsible for period changes and the reliable determination of the absolute parameters of the eclipsing pair.

2. New observations

2.1. Photoelectric photometry

The first set of photoelectric observations of XY UMa was obtained at the Skalnaté Pleso (SP) and Stará Lesná (SL) Observatories of the Astronomical Institute of the Slovak Academy of Sciences. The system was observed over 45 nights from December 31, 1997 to November 5, 2000. At both observatories a single-channel pulse-counting photoelectric photometer installed at the Cassegrain focus of the 0.6 m reflector was used. Observations at SP were carried out through the standard *BVR* filters using the photomultiplier HAMAMATSU R 4457P sensibilised in the *R* passband. The standard *UBV* filters were employed at SL using the photomultiplier EMI 9789 QB. The integration time of one measurement was 10 seconds. SAO 27151 and GSC 167-3805 (check star of Hilditch & Bell 1994, hereafter H&B) served as a comparison and check star, respectively. Both components of SAO 27151 were well inside the diaphragm of the photomultiplier. The check star was found to be stable within 0.02 mag in the *V* passband. The average standard error of one observation during clear nights reached 0.015 mag in *U*, 0.009 mag in *B* and 0.008 mag in *V* and *R* passbands. The rather large error in the *U* passband is caused by the late spectral type of the variable star and low sensitivity of both photomultipliers in the ultraviolet region. The data were transformed to the international *UBV* system in the usual ways. Simultaneous observation of XY UMa on February 5, 1998 showed that the differences in the standard *UBV* magnitudes obtained at both observatories are lower than 0.01 mag.

The second part of the photoelectric photometry was obtained using the San Diego State University 61-cm telescope at Mt. Laguna. XY UMa was observed over 38 nights from February 26, 1994 to May 27, 2000. The telescope is equipped with a photometer using a HAMAMATSU R943-02 tube cooled to −15°C. The *BVRI* filters were chosen to closely match the Johnson-Cousins system. One observational point consists of two 20-second integrations. The comparison star SAO 27139 was used for all observations of XY UMa. The observations were transformed into the international *BVRI* system using the Landolt (1973, 1983) standard stars. The total number of observations obtained at both observatories in the *V* passband exceeds 8200.

Previous investigators used as many as 5 comparison and 2 check stars. This makes the analysis of the long-term brightness variations of XY UMa difficult (the finding chart of all stars is shown in Fig. 1). Therefore,

Table 1. *BV* magnitudes of all comparison stars used in both our and previous studies. For the variable we give the maximum brightness in the last observing season. The standard errors are given in parentheses. For example, the entry 9.596(9) should be interpreted as 9.596 ± 0.009. *BV* magnitudes of S1 and S2 correspond to both components of the visual pair

No.	BD/GSC	SAO	*V*	*B*	Sp.
1	+55°1320	27151	9.596(8)	10.051(7)	F8
2	+55°1321	27153	9.423(6)	9.544(8)	A0
3	3805-167	–	10.633(3)	11.055(3)	-
4	+54°1278	27139	9.542(6)	9.945(5)	F5
5	+55°1314	–	9.439(5)	10.436(3)	-
var.	+55°1317	27143	9.41	10.24	K0?

on December 1, 2000 we remeasured the brightness of all comparison stars used by previous authors (see Table 9). The magnitudes were determined using standard stars in the Praesepe cluster which is located about 35° from XY UMa. The measurements of standard stars were performed on a large range of the air masses to ensure reliable determination of the extinction coefficients. The consistency of the transformation to the international UBV system was checked on the standard extinction star 26 UMa ($V = 4.50$, $B - V = 0.00$, $U - B = 0.04$, Henden & Kaitchuck 1982). The magnitudes of the Praesepe standards determined using 26 UMa showed only slight dependence on the spectral type. The B and V magnitudes of standards were within 0.01 mag of the published values. The U magnitudes exhibited a systematic shift of -0.04 mag. Therefore in Table 1 we give only the resulting B and V magnitudes. The brightness of S1 and S2 refers to the combined light of both visual components fitting safely into the photometer diaphragm. According to our measurements, SAO 27139 is 0.052 mag brighter than SAO 27151. The opposite result ($\Delta V = -0.07$) of H&B is rather surprising. Hence observations with respect to S1 (and S2) must be taken with caution and systematic shifts as large as 0.12 can be expected.

Since the orbital period of XY UMa is about 11.5 hours, we have not succeeded in covering a complete LC in one night. Therefore, observations from the subsequent nights in time intervals not exceeding two months were used to construct the complete LCs. The journal of observations is given in Table 2. The resulting LCs in the V passband are shown in Fig. 2. The data are phased using linear ephemeris determined from all primary minima since JD 2 449 400 (February 1994):

$$\text{Min } I = \text{HJD}2\,435\,216.3963 + 0.47899824 \times E. \quad (1)$$

Small differences between the LCs obtained in individual nights enlarge the scatter of the complete LCs. This is the case mainly for the LCs obtained at SP and SL, were the complete LCs were usually constructed from longer time intervals than at ML. The observed LCs show only slight night-to-night variations in all passbands. Individual observations can be obtained via ftp from `cdsarc.u-strasbg.fr`.

Our observations led to the determination of 27 primary and 16 secondary minima times. They have been calculated separately for each passband using Kwee & van Woerden's (1956) method. Some of them were already published (C&P and Pribulla et al. 1999a). The observations performed at ML usually have insufficient coverage of minima during individual nights. Hence we have constructed composite phase LCs using mean linear ephemeris (1) valid since 1994. Thereafter, the positions of minima in phase diagrams were transformed to normal minima times (close to the JD_{mean} in Table 2). Our minima times (together with those published previously) are listed in Table 4.

Table 2. Journal of the new photoelectric observations obtained at the Mount Laguna (ML), Skalnaté Pleso (SP) and Stará Lesná (SL) observatories. JD_{mean} are arithmetic means of HJD times of the individual observations in the V passband. LC 17 was not used for determination of the photometric elements and spot parameters

LC	Dates	JD_{mean} 2400000+	Obs.
01	Feb. 26,28, Mar. 1,2,4, 1994	49413	ML
02	Feb. 7,11,12,20,24,26, 1995	49768	ML
03	May 5,6,7,9,10,12,13, 1996	50213	ML
04	Dec. 31, 1997, Jan. 1,23,25, Feb. 5,7, 1998	50833	SP,SL
05	Feb. 23, Mar. 15,30, 1998	50883	SP,SL
06	May 16,20,24,27,28, 1998	50956	ML
07	Nov. 12, 23, Dec. 2,10, 1998	51148	SP,SL
08	Dec. 29, 1998, Jan. 4, 1999	51179	SP
09	Jan. 17,21,24, 1999	51201	SP,SL
10	Feb. 27, Mar. 12,13,18, 1999	51246	SP,SL
11	Apr. 4,5,9, 1999	51276	SL
12	May 14,19–21,24–28, 1999	51322	ML
13	Nov. 15, Dec. 5,16,17,21, 1999	51521	SP,SL
14	Dec. 31, 1999, Jan. 6,16, 2000	51549	SP,SL
15	Feb. 27, Mar. 13,22, Apr. 9, 2000	51617	SP,SL
16	May 18,19,21,22,25,27, 2000	51687	ML
17	Oct. 15,20,27,29, Nov. 5, 2000	51846	SL

2.2. Spectroscopy

Our XY UMa spectra were taken from January 8 to 10, 1998 and on the night January 5/6, 1999 by the 1.82-m Asiago telescope, using the Reosc Echelle Spectrograph (RES) equipped with a CCD detector. The RES dispersion varied from 5 Å mm^{-1} (4330 Å) to 10 Å mm^{-1} (6840 Å) for 1998 spectra and from 6.3 Å mm^{-1} (4100 Å) to 13.7 Å mm^{-1} (9050 Å) for 1999 spectra. The exposure time of 20 min was employed for all spectra. The journal of observations is given in Table 3. The RES echelle

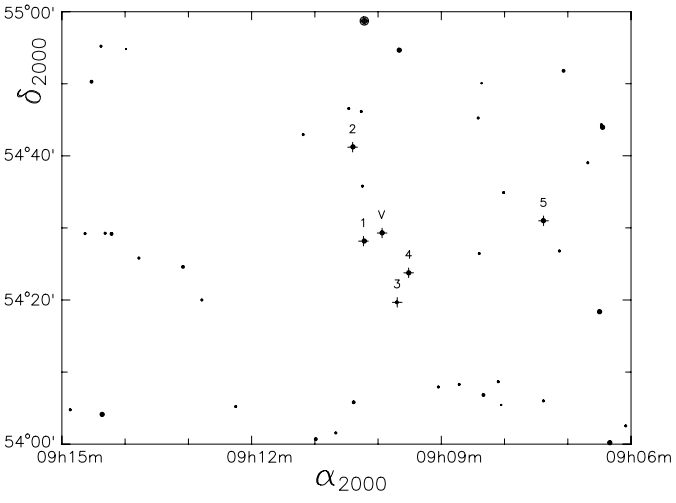

Fig. 1. The finding chart of XY UMa (denoted by V) and all comparison stars used by previous observers (corresponding to Table 1)

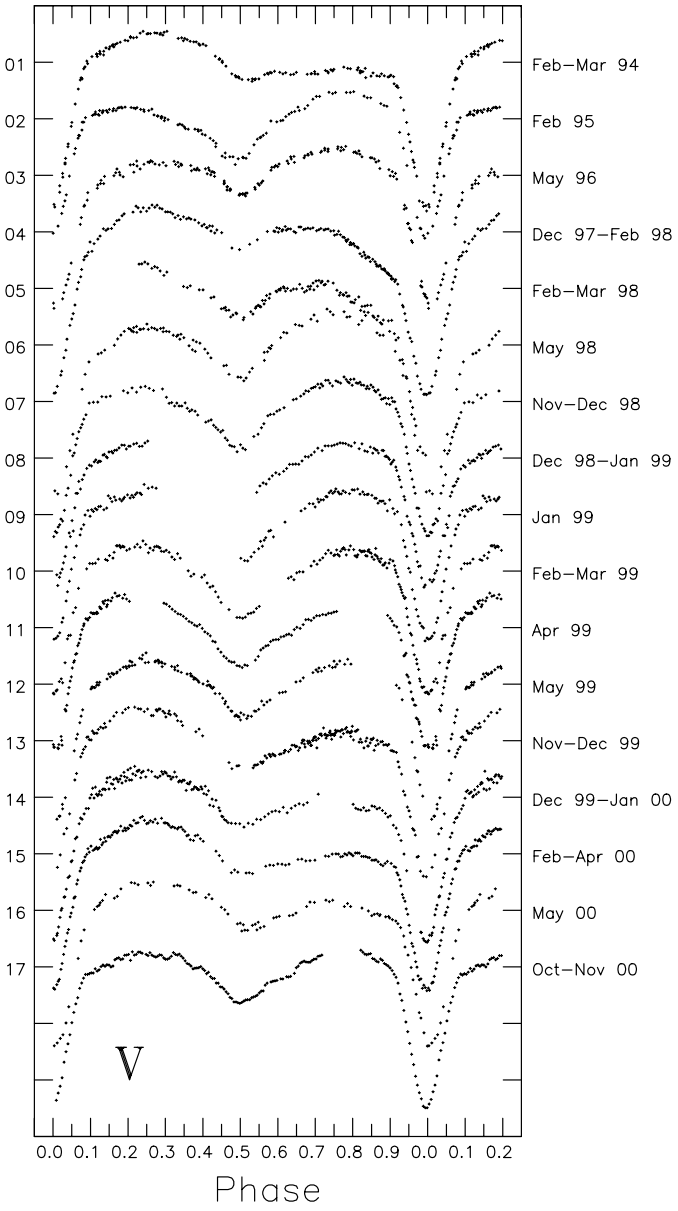

Fig. 2. V light curves of XY UMa (corresponding to Table 2)

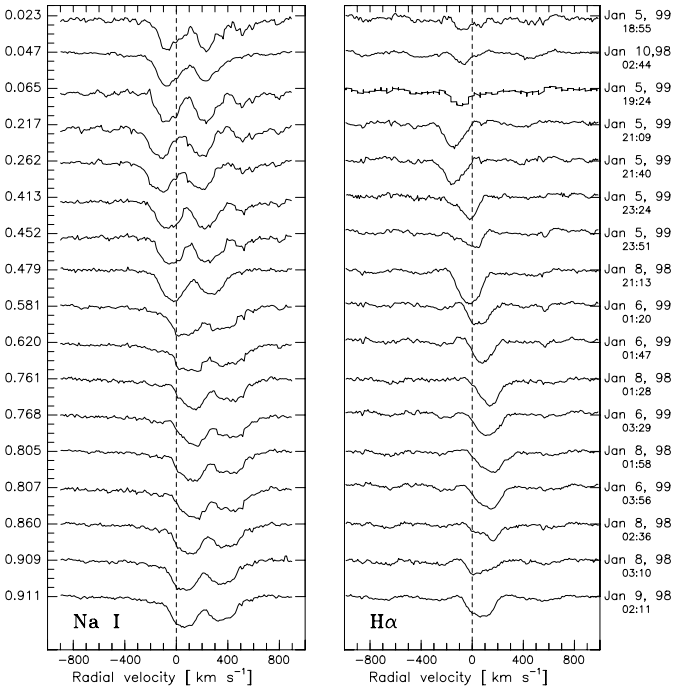

Fig. 3. The Na I D and H_α line profiles stacked in a phase sequence. The spectra are shifted in intensities by 0.4 relative to one another

orders were straightened through dedicated software developed at the Astronomical Observatory of Capodimonte in Naples. Thereafter, the spectroscopic data were processed using the following steps: (1) flat-field correction and bias subtraction; (2) sky-background subtraction; (3) calibration in wavelength using a thorium lamp for comparison lines; (4) correction to the heliocentric velocity; (5) normalization to continuum (equal to 1); (6) removal of cosmic ray spikes. All of the procedures were carried out using the ESO MIDAS reduction software.

During the 1998 observing run we did not perform observations of the standard stars. The consistence of our *RV*s was tested using 10 telluric absorption lines in the range 6867–6882 Å. Their mean *RV* was $+1.0\pm0.6$ km s^{-1}.

During the 1999 observing run we obtained also the spectra of the IAU *RV* standard star 43 Tau. Medeiros & Mayor (1999) give its spectral type as K2III, $(B-V) = 1.07$, radial velocity $V_\mathrm{r} = 24.39 \pm 0.26$ km s^{-1} and rotational velocity $v \sin i < 1$ km s^{-1}. The spectra of the comparison star were reduced in the same way as the spectra of XY UMa. The *RV* of 43 Tau has been determined from the 30 strongest Fe I, Ca I and Ti I lines covering most of the echelle orders. The resulting *RV* (after the heliocentric correction) is 23.7 ± 0.8 km s^{-1} within the error of the published value. Hence our system is shifted less than 1 km s^{-1} with respect to the international system. The S/N ratio for our spectra was 100–140 around H_α.

3. Analysis of the spectroscopic data

Our spectra of XY UMa are dominated by the rotationally broadened absorption profiles of the primary component. According to Huisong & Xuefu (1987) its rotational velocity is about 100 km s^{-1}. The lines of the secondary component are scarcely visible in the Ca II infrared triplet around the quadratures. We tried to estimate the spectral type of the primary component from the intensity of the temperature-sensitive Mg I 5172 Å line using the spectrum taken during the secondary eclipse (phase 0.479), when the light contribution of the secondary component was negligible. The derived effective temperature $T_\mathrm{eff} = 5300$ K indicates the spectral type K0V, in disagreement with widely accepted G3V spectral type. The spectral classification based on the Balmer lines is biased by the presence of photospheric emissions formed in the active regions, which

Table 3. Journal of the spectroscopic observations of XY UMa and mean radial velocities of the primary component determined from the metallic lines. UT times correspond to mid-exposures. Phases were computed according to ephemeris (1)

No.	Date	UT	JD_{hel} 2450000+	Phase	*RV*
01	Jan. 8, 1998	01:28	821.5655	0.761	136.5
02	Jan. 8, 1998	01:58	821.5864	0.805	126.9
03	Jan. 8, 1998	02:36	821.6128	0.860	102.2
04	Jan. 8, 1998	03:10	821.6364	0.909	72.2
05	Jan. 8, 1998	21:13	822.3885	0.479	−12.1
06	Jan. 9, 1998	02:11	822.5955	0.911	69.5
07	Jan. 10, 1998	02:44	823.6184	0.047	−54.4
08	Jan. 5, 1999	18:55	1184.2926	0.023	−44.6
09	Jan. 5, 1999	19:24	1184.3127	0.065	−63.0
10	Jan. 5, 1999	21:09	1184.3856	0.217	−124.1
11	Jan. 5, 1999	21:40	1184.4072	0.262	−126.7
12	Jan. 5, 1999	23:24	1184.4794	0.413	−57.0
13	Jan. 5, 1999	23:51	1184.4982	0.452	−32.7
14	Jan. 6, 1999	01:20	1184.5599	0.581	39.8
15	Jan. 6, 1999	01:47	1184.5787	0.620	59.4
16	Jan. 6, 1999	03:29	1184.6495	0.768	119.6
17	Jan. 6, 1999	03:56	1184.6683	0.807	121.3

reduce the observed equivalent widths. The whole problem of the spectral classification using the stellar atmosphere models is beyond the scope of the present paper and will be postponed for future investigation.

3.1. Line profiles variations

The spectra taken in 1998 and 1999 overlap in the wavelength region 4500–6700 Å. The line profiles of two important absorption lines in this range H_α and Na I D doublet are shown in Fig. 3. The most interesting are H_α line profile changes. For instance, the absorption line profile taken just before the primary minimum on January 8, 1998 (the phase 0.909) is deformed by the short-lived emission feature (seen also in the previous spectrum in the phase 0.860), which disappeared on the subsequent night (the phase 0.911) and is probably connected to chromospheric activity. This fast variation, however, is not seen in the Na I D doublet. On the other hand, the H_α profile at the phases 0.805 and 0.807 did not change in the course of a year. The opposite is the case for the phases around the secondary minimum – the spectral lines in phase 0.452 taken in January 1999 show only shallow absorption compared to the spectrum in phase 0.479 taken in January 1998. This corresponds to the LCs observed almost simultaneously (LC4 and LCs 8,9). While LC 4 shows a shallow secondary minimum and depressed ingress to the primary minimum, LCs 8 and 9 display equal maxima and the deep secondary minimum. This behaviour can be explained by a large cool starspot facing the observer at the secondary minimum in January 1998. The line profiles observed in phases 0.023, 0.047 and 0.065 are deformed by the Rossiter-McLaughlin effect. We can conclude that the shape of the H_α profile is controlled by the interplay of the short-lived chromospheric activity with the long-term maculation effects.

3.2. Radial velocities of the primary component

The *RV*s of the primary component were determined by the parabola fitting of the Doppler cores of the 30 strongest metallic lines, since the Balmer absorption lines are affected by the chromospheric activity. The standard error of the mean *RV*s do not exceed 5 $\mathrm{km\,s^{-1}}$. Resulting *RV*s are shown in Fig. 4 together with all published data. The *RV*s of Kjurkchieva et al. (2000) were determined by scanning their Fig. 7. The error of the retrieved data did not exceed 0.8 $\mathrm{km\,s^{-1}}$. The authors used old linear ephemeris for phasing the data, which is clearly seen in their *RV* curve. Therefore we shifted their data by −0.0467 to obtain an agreement with our new ephemeris valid throughout their observations. Moreover, the authors did not observe any standard *RV* stars, so the V_0 shift of their *RV*s in comparison with previous investigations is most probably only an instrumental effect. From Fig. 4 it is seen that our *RV* observed at the orbital phase 0.761 deviates much from the general course of the data. This is probably caused by the spot positioned on the primary facing the observer before the primary minimum (see Table 9). This *RV* was neglected from our analysis. We have also neglected *RV*s determined during the primary eclipse. These cannot be used for the *RV* determinations in the mass-point approximation since the profiles are clearly deformed by the Rossiter-McLaughlin effect.

Since both datasets (1998 and 1999) were obtained using the same spectrograph, the *RV*s were combined to find the spectroscopic elements of the primary component. The sinusoidal fit of the data provides $K_1 = 123.6 \pm 3.0\ \mathrm{km\,s^{-1}}$, $V_0 = -0.9 \pm 2.1\ \mathrm{km\,s^{-1}}$ and the mass function $f(m) = 0.094 \pm 0.007\ M_\odot$. The resulting elements are somewhat different from the values published by Pojmanski (1998). The errors of our spectroscopic elements are larger due to the lower quality and quantity of the data. The semi-amplitude of the *RV*s of the primary component is larger due to the maculation effects present during both observing runs. The spectroscopic observations in 1998 and 1999 correspond to the photoelectric LC 4 and LCs 8-9, respectively. The influence of the maculation effects on the determined *RV*s was assessed using the spot parameters obtained by the LC fitting (Table 9). The dark spot facing the observer before the primary minimum (LC 4) causes an increase ($\approx$5 $\mathrm{km\,s^{-1}}$) of the *RV* around the maximum II and explains the larger semi-amplitude of K_1. On the other hand, in 1999 one of the spots facing the observer during the secondary minimum (LCs 8 and 9) did not affect the *RV* curve. Tests with synthetic *RV* curves corresponding to the observed spot positions (Table 9) show the scatter in K_1 to be equal to $\pm 2.4\ \mathrm{km\,s^{-1}}$ and in V_0 equal to 0.9 $\mathrm{km\,s^{-1}}$. For the reliable determination of the "clean" spectroscopic elements one has to perform simultaneous fitting of the radial velocities (or line profiles) with

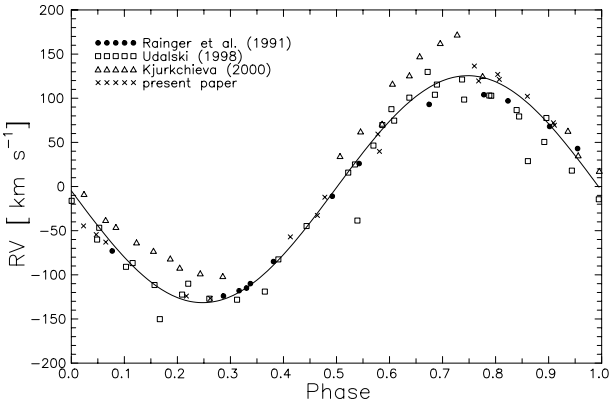

Fig. 4. Radial velocities of the primary component of XY UMa and the best sinusoidal fit to our data

photoelectric LCs including the maculation effects covering the full orbital cycle. Our spectroscopic data do not meet these requirements. Therefore, we will accept the spectroscopic elements published by Pojmanski (1998) for the rest of the present paper.

It is interesting to note the large discrepancy in V_0 between the different sets of data. If this is real, it can be caused by another body in the system with the orbital period of a few years, as in the system AW UMa (Pribulla et al. 1999b). Further spectroscopic observations are necessary to prove or exclude this possibility.

4. Period study

Our period analysis is based on all available photographic and photoelectric minima times. The primary minima times prior to 1990 were weighted according to P&G with w ranging from 0 to 16. The weight $w = 16$ was used for recent minima times because of their higher precision. The visual minima times, used by Kjurkchieva et al. (2000), were neglected since their scatter obscures the (O–C) diagram.

The list of published minima times was augmented by four values determined from the high-precision CCD photometry kindly provided by Dr. Hilditch (see Hilditch & Collier Cameron 1995). One unpublished time of the minimum determined from the Hipparcos photometry was communicated by Prof. Kreiner (2000). We also determined the normal times of one primary and one secondary minimum from Fig. 1 of Lee (1993) by transforming the *UBV* LCs to machine-readable form and using the ephemeris applied by the author for phasing the LCs.

The complete list of the minima times is given in Table 4. They are appended by the differences in corresponding brightness maxima (in magnitudes):

$$\Delta M = \text{Max II} - \text{Max I}, \quad (2)$$

as suitable measures of the LCs asymmetries. Most of the data were taken from P&G. The rest of the differences were determined by fitting the maxima by parabolae as described in Sect. 5.

The (O–C) diagram for all minima, constructed using the mean linear ephemeris, is displayed in Fig. 5. The (O–C) residuals for the primary minima clearly show a wave-like behaviour.

The period analysis of XY UMa is complicated by an enhanced photospheric activity of the components, seen as the variations in the levels of the minima and maxima. Additional light caused by the presence of the bright or/and dark spots causes apparent shifts of the minima. This affects mainly the position of the secondary minimum which is sometimes indeterminable (e.g., LC 15, Fig. 2). For this reasons we have not taken into account the secondary minima times in the further analysis (see P&G).

4.1. The third body in the system

The presence of a third body has been tested by a correlation analysis of the minima and differences of the maxima height (P&G). The authors obtained two possible orbital periods ($P_3 = 24$ or 40 years) of the third body to get a nearly perfect correlation of the (O–C) residuals and maxima differences. C&P conclusively determined the orbital period of the third body as 30.5 years. On the other hand, Kjurkchieva et al. (2000) claimed that the apparent period changes are caused by the LC asymmetries alone.

We augmented the dataset of P&G by 43 new minima and corresponding differences of the maxima height. To ascertain the reality of the third-body orbit we have used only primary minima and normal epochs determined from the old photographic data by C&P. From this dataset we have chosen only minima determined from the LCs with a certain degree of asymmetry (difference of the maximum height less than 0.002, 0.004 mag and so on). It is obvious that the number of available minima increases with the allowed maximum asymmetry. Each subset of data was fitted separately to yield the elements of the third body by the differential correction method with the period of the binary system not fixed (for details see C&P). The solution did not converge for the most symmetric minima ($\Delta M < 0.01$ mag), due to the small number of data points. The first stable solution was attained for 47 minima determined from the LCs with asymmetries less than 0.016 mag. The dependence of the orbital period P_3 and semi-major axis $a_{12} \sin i$ on ΔM was weak. The third-body orbit is sufficiently defined by minima determined from almost symmetric LCs. Hence, the deviations of the minima from the mean linear ephemeris cannot be explained only by LC asymmetries.

The third-body fits for the primary minima determined from almost symmetric LCs ($-0.016 < \Delta M < 0.016$) and all minima are shown in Fig. 5. The primary minima with different asymmetries are denoted separately (see the legend). One can see that minima with $\Delta M > 0.016$ mag and $\Delta M < -0.016$ mag are positioned mainly above and below the third-body fits, respectively. This is best seen from the data obtained since 1993.

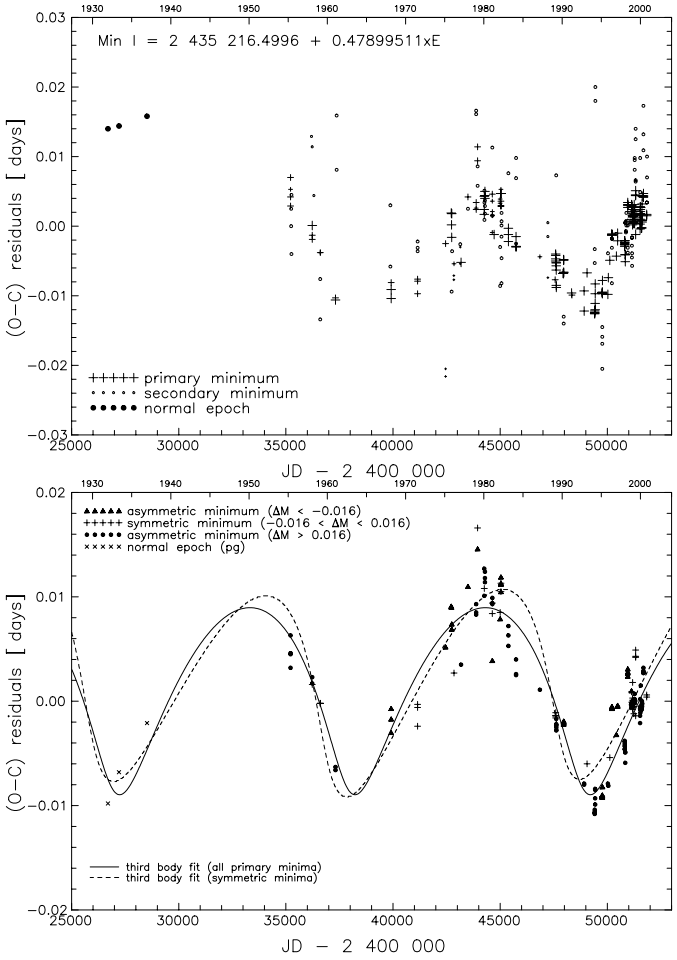

Fig. 5. The (O–C) residuals for all minima times from the mean linear ephemeris. The weights of the primary minima correspond to their size (top). The (O–C) residuals of the primary minima with non-zero weights from the optimal quadratic ephemeris and the best third-body fit for all minima (corresponding to the elements given in Table 5) and minima from most symmetric LCs with $|\Delta M| < 0.016$ (bottom)

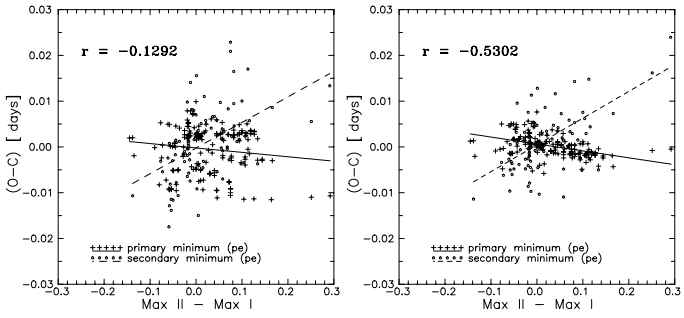

Fig. 6. Correlation of the differences of the maxima brightness (ΔM) and (O–C) residuals from the mean linear ephemeris (left) and the third-body fit for all primary minima (right)

The full scatter of times of minima caused by the LC asymmetries is also clearly visible.

The reality of the third body was also tested by correlation analysis of the residuals. The correlations of the (O–C) residuals from the linear ephemeris and the third-body orbit and corresponding differences in maxima height are shown in Fig. 6. We have rejected from this analysis all minima with the zero weight as given by P&G and minima with unknown ΔM. The primary and secondary minima were treated separately for obvious reasons.

Table 5. The light-time effect solution and corresponding ephemeris of the binary system. $T_{\rm super}$ and $T_{\rm infer}$ are the times of the superior and inferior conjunction of the third body, respectively

Element			σ
$P_{\rm third\ body}$	[years]	30.09	0.41
e		0.47	0.07
ω	[°]	250	10
T_0	[JD]	2 437 880	310
$a_{12} \sin i$	[AU]	1.58	0.08
$f(m_3)$	[$M_\odot$]	0.0043	0.007
$T_{\rm super}$	[JD]	2 449 050	330
$T_{\rm infer}$	[JD]	2 444 680	790
JD_0	[JD]	2 435 216.4997	0.0007
$P_{\rm binary}$	[days]	0.47899425	$6\ 10^{-8}$
Q	[days]	$2.72\ 10^{-11}$	$0.19\ 10^{-11}$
$\sum$(O–C)^2	[days^2]	0.011639	-

One can see that there is almost no correlation ($r = -0.129$) for the primary minima for the case of the constant period, while (O–C) residuals correlate rather tightly for the case of the third body ($r = -0.530$). The resulting relations between the (O–C) residuals (ΔT) from the third-body fit and differences in the maxima height (ΔM) in the case of the primary and secondary minima are:

$$\begin{aligned} \Delta T^{\rm pri} &= \underset{\pm 21}{-0.00173}\ \underset{\pm 16}{\Delta M - 0.0008} \\ \Delta T^{\rm sec} &= \underset{\pm 10}{0.058}\ \underset{\pm 8}{\Delta M + 0.0004.} \end{aligned} \qquad (3)$$

These results are in accord with the expected deviations of minima caused by one spot positioned on a hemisphere facing the observer around quadratures. The Fourier period analysis of the (O–C) residuals in the range 100–3000 days gave the best period, 695 ± 17 days, which is within the error of the 709 ± 10 day periodicity found in the maximima height differences ΔM (see Sect. 5).

The resulting elements of the third body determined from all primary minima are given in Table 5. If we assume the total mass of the eclipsing pair $m_1 + m_2 = 1.76\ M_\odot$, we will obtain the minimum mass of the third body $m_3 = 0.26\ M_\odot$ for $i_3 = 90°$. In this case the total mass of the triple system provides the semi-major axis of the third body from the eclipsing pair $a_{123} = 12.2$ AU. Assuming the Hipparcos distance of XY UMa $d = 66$ pc, we get the angular separation of the third body from the eclipsing pair as $0.18''$. The expected half-amplitude of the systemic velocity changes of the eclipsing pair, 1.77 km s^{-1}, is comparable to the precision of the systemic velocity determination.

4.2. Applegate's mechanism

A long-term wave-like variation of the minima can be also explained by the action of Applegate's mechanism, first proposed for XY UMa by Henry et al. (1995). Erdem & Güdür (1998) accepted this possibility as a suitable explanation for the long-term period and brightness changes of the system. Lanza & Rodonò (1999) included XY UMa to their list of 46 close binaries displaying magnetic modulation of the orbital period. The reality of this explanation has not been reliably tested yet.

Erdem & Güdür (1998) noted that the maximum and minimum system brightness does not coincide with the maximum and minimum of the (O–C) curve. C&P scaled the amplitudes of the (O–C) residuals and the mean maximum visual brightness:

$$V_{\max} = (\mathrm{Max\ I} + \mathrm{Max\ II})/2 \qquad (4)$$

of XY UMa. Their Fig. 3 indicates that there is no correlation or anticorrelation between these two datasets.

In the present paper we will ascertain the reality of this mechanism in XY UMa quantitatively by the correlation analysis of the (O–C) residuals and the mean maximum visual brightness. The $V_{\max}$ is directly proportional to the visual luminosity of the primary component, since in quadratures, uneclipsed hemispheres of both components are seen and the contribution of the secondary component to the luminosity of the system is very small. Another indicator of the magnetic period modulation is the $(B-V)_{\max}$ colour index which should correlate or anticorrelate with the maximum brightness (see Applegate 1992). Unfortunately, the B passband observations are rather scanty. Moreover, the differences between the instrumental and standard B magnitudes are significant. The historical $V_{\max}$ and $B_{\max}$ magnitudes of XY UMa were determined from all available LCs by parabola fitting (see Sect. 5). Thereafter, the magnitudes were standardised using the B and V magnitudes of comparison stars from Table 1. For every available LC, the normal minimum time (*NMT*) from adjacent primary minima times was determined. Thereafter, the (O–C) residuals from the mean linear ephemeris were calculated for the *NMT*. Figure 7 shows the comparison of these residuals, NMT_{res} and $V_{\max}$ for both datasets. The resulting correlation coefficients $r(V_{\max}, NMT_{\mathrm{res}}) = 0.134$ and $r((B-V)_{\max}, NMT_{\mathrm{res}}) = 0.282$ do not support the reality of the mechanism.

4.3. Discussion

The observed (O–C) diagram is the superposition of the LITE and the deviations caused by the asymmetries of the minima determined from spotted LCs. Slight long-term increase of the period of the system can be invoked to explain the data in terms of the isotropic mass loss from the system by the stellar wind and/or by the LITE caused by another body on the long-period orbit.

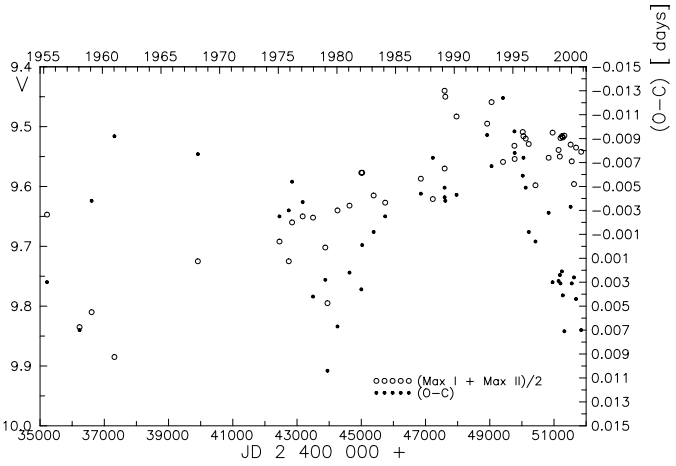

Fig. 7. Comparison of the visual brightness of XY UMa in maxima and (O–C) residuals from the mean linear ephemeris for normal epochs

5. Brightness and colour of the system

The maximum visual brightness as well the $(B-V)$ colour index of XY UMa are known to vary. Geyer (1976) noted that the average brightness of the system increased from 1955 to 1975 by about 0.18 mag in V filter. He also noted additional variations over short time scales. The complete photometry performed by Geyer was analyzed by Lee (1985). Jeffries (1995) compiled the visual magnitudes of the LC extrema from 1955 to 1995. He standardised the differential magnitudes for observations with SAO 27151 as the comparison star to Δmag with respect to the more commonly used SAO 27139. The resulting dataset shows a definite trend: XY UMa has been getting brighter in a phase-independent way. Hilditch & Collier Cameron (1995) explained this by changes in the area of the high and low latitude spots visible both in and out of the eclipse.

The results of such compilations should however be taken with caution, due to misprints (see C&P), misidentifications of the comparison stars, non-conformity of the photometric systems with the international Johnson *UBV* system, etc. The average maximum brightness of XY UMa in the 90 s was about $V_{\max} = 9.5$ (see Fig. 8). The V passband LC of Kjurkchieva et al. (2000) gives $V_{\max} = 8.85$! Their original observations (in Δmag), kindly provided by Dr. Marchev, and our determination of the brightness of their comparison star SAO 27153 (see Table 1), led to $V_{\max} = 9.60$. Zeilik et al. (1988a) probably displayed in their Figs. 1–4 ($-\Delta$mag) of XY UMa with respect to its maximum brightness instead of magnitude differences, as given in the text, since no comparison star has the same colours as XY UMa.

Most observers used SAO 27139 (S4) as the principal comparison star (see Table 8). In several cases SAO 27151 and SAO 27153 were also used. Most published data were left in the instrumental system. Hilditch & Collier Cameron (1995) estimated the differences between instrumental and international systems in the V passband for

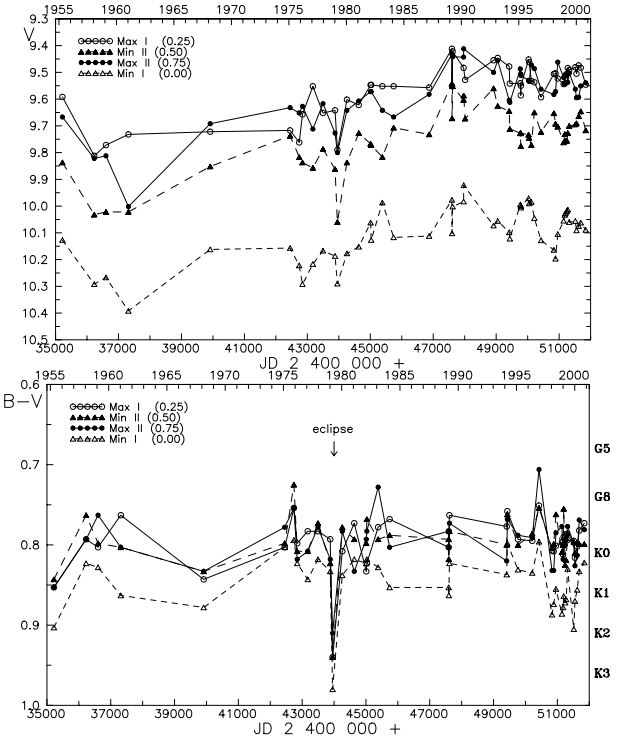

Fig. 8. Historical visual brightness and the $(B-V)$ colour index of XY UMa. The eclipse of XY UMa by the possible protostellar body in the system is marked by the arrow

the published measurements to be <0.02 mag. The authors, however, did not take into account real differences in filter transparency and photomultiplier response.

The standartising of the observed magnitudes obtained in strictly differential photometry is performed using the following equation (see e.g., Henden & Kaitchuck 1982):

$$\Delta V \ = \Delta v \ - k_V(X_{\rm comp} - X_{\rm var}) + \varepsilon\Delta(b-v), \qquad (5)$$

where Δv and ΔV are observed and standard magnitude differences of the variable and comparison star, k_V is the extinction coefficient in the V band, $X_{\rm comp}$ and $X_{\rm var}$ are the air masses of the comparison and variable star, $\Delta(b-v)$ is the colour difference of the variable and comparison star and ε is the transformation coefficient from the instrumental to the international system. The extinction correction is practically negligible since the comparison stars are very close to XY UMa. In the case of SAO 27139, the angular distance is about $6'$. For a maximum reasonable zenith distance of 60° and a typical extinction coefficient $k_V \approx 0.3$, the correction does not exceed 0.002 mag. The last term of the Eq. (3) is, however, much higher. The magnitude difference of the variable and comparison star Δm_λ at a given wavelength λ (in nm) can be estimated as follows:

$$\Delta m_\lambda = \Delta m_V + (550-\lambda)\frac{(\Delta m_V - \Delta m_B)}{550-440}, \qquad (6)$$

where m_V and m_B are magnitude differences in the V and B passband, respectively. Effective wavelength of the measurement depends on the spectral response of the photomultiplier and effective wavelength of the filter. In an extreme case, Jeffries (1995) used instrumental V filter with $\lambda_{\rm eff} = 525$ nm and the comparison star S1. From the above equation we get a difference between his instrumental and the international system of 0.08 mag!

Hence, the published brightness of XY UMa has to be taken with caution and differences as large as 0.05 mag should be expected.

To ascertain long and short-term changes of the brightness of XY UMa we have determined the brightness in the LC extrema for all published LCs in ±0.05 phase intervals by parabola fitting. Some LC extrema were determined from the original observations provided by the authors. In a few cases, the LCs were obtained by scanning the published figures and transforming the pixel coordinates appropriate to the centers of the symbols to phases and magnitudes as described in Pribulla et al. (2000). The resulting visual brightness and $(B-V)$ colour index in the LC extrema is displayed in Fig. 8. The data from Pojmanski & Udalski (1990) showing rather low colour index $(B-V \approx 0.6)$ were omitted.

The spectral type of the primary component, corresponding to the observed $(B-V)$ colour index (sequence taken from Popper 1980), varies from G8 to K1 during the eclipse of the secondary component. This is in disagreement with the widely accepted spectral classification of G3V (Strassmeier et al. 1993). The colour excess of XY UMa might be caused by the presence of other components or by an absorbing circumstellar cloud.

It is obvious (see Fig. 8) that the maximum brightness has been increasing steadily since 1961. This trend has been interrupted by a definite decrease in 1979, interpreted by C&P as a partial eclipse of the eclipsing pair by a protostellar third body. The dip in the V passband was accompanied by the reddening in the $(B-V)$ colour index corresponding to K2-3 spectral type. The course of visual brightness of XY UMa still has not progressed through one cycle.

The long-term brightness variability is accompanied by the faster changes in the asymmetry of the LCs. To determine whether these changes are cyclic and coherent we performed a Fourier period analysis of the differences of the maxima height (Max II – Max I), which are less affected by discrepancies in the instrumental systems. The resulting power spectrum in the interval 100–3000 days gives the best period of 709 ± 10 days. Since the period is close to two years and XY UMa can be observed only from October to May, the symmetric LC should repeat in two or three observing seasons while asymmetry of the LC should change in the opposite way from season to season. The first phenomenon is supported by observations in spring 1988, 1989 and 1990 when the LC remains fairly symmetric. The second behaviour is obvious from the LCs obtained in the spring of 1994 and 1995. Our LCs obtained since 1994 do not support this behaviour fully. Above all, the phase diagram of the maxima differences with the 709-day periodicity shows a few observations not conforming to the general trend of the data. The above phenomenon is probably only quasi-periodic and the possible 709-day periodicity requires further observational evidence.

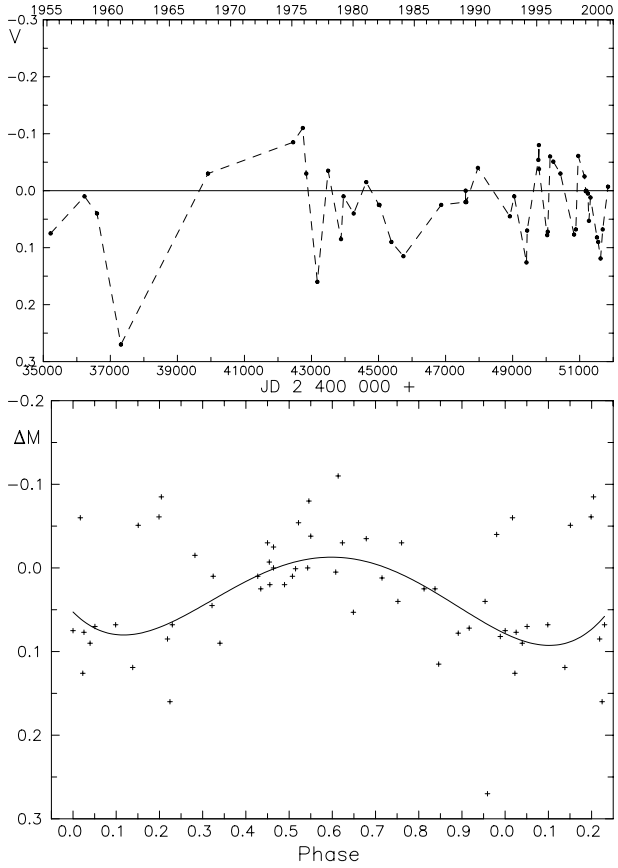

Fig. 9. Differences in the maxima brightness ΔM (top). The quasi-periodic variation is clearly visible in the recent data. The phase diagram for the possible 709-day quasi-periodicity (bottom). The fit is schematic

A reliable determination of the brightness of the system suitable for this analysis will require that all observations be performed in the standard Johnson system with respect to the same sufficiently stable comparison star. With the possibility of future improvements of the *UBV* magnitudes of the comparison stars, one should *publish or archive* differential magnitudes with the heliocentric Julian dates.

6. Photometric elements

The problem of finding reliable "clean" photometric elements from spotted LCs is very difficult. As shown by the IUE spectroscopy (Budding et al. 1982), XY UMa binary is the most active member of the short-period RS CVn-like group. Its LC undergoes variations as large as 0.2 mag. It is impossible to observe an unspotted LC. In spite of this, there is a usual practice to regard symmetric LCs as unspotted. Budding & Zeilik (1987) claimed to separate spot effects from eclipse effects and stated that "clean" elements should not vary with time. Banks & Budding (1989) have admitted the inadequacy of the method. Fitting of the spotted LC does not remove spot effects correctly. The method is especially defective for symmetric LCs, when the spots are positioned on the hemispheres facing the observer around the minima. This fact is reflected in the preferred quadrature position of the spots in many active binaries, leading to incorrect conclusions about the presence of active longitude belts (RT And – Zeilik et al. 1989; SV Cam – Zeilik et al. 1988b). However, despite the unreliability of the spot determination, the "clean" geometric elements depend significantly on the type of asymmetry. Insufficient coverage of the solved LCs also affects the determination of the correct elements (H&B). The fitting of the spotted LCs by any of the present methods is inadequate.

Table 6 summarizes published geometric elements. The type of radius has often not been specified (polar, equatorial, mean etc.). Published surface potentials (or $r_{\rm back}$) were transformed to mean fractional radii to make the results comparable. Temperatures of the primary (5700–5800 K) were set according to the spectral type. Due to the fact that the determined parameters show substantial differences, the geometrical elements i, r_1, r_2 of XY UMa are virtually unknown. Hence, the exact position of the spots found in the literature (e.g., Kjurkchieva et al. 2000) are disputable. On the other hand, Collier Cameron & Hilditch (1997) sought the combination of geometric parameters to get best simultaneous fits of 1992 October and 1995 November LCs. The resulting parameters $i = 81°$ and $r_2 = 0.66\ R_\odot$ are in good agreement with those obtained from the 1992 data alone (H&B). The authors, however, had at their disposal only V passband observations.

In our approach, we propose to form a clean LC by combining a large number of the observed LCs. The clean LC is then defined by the maximum brightness of a binary in every phase bin. This method was successfully applied to RT And (Pribulla et al. 2000). The situation with XY UMa is complicated by the intrinsic changes of the maximum brightness. The mean maximum brightness of the system ((Max I + Max II)/2) seems to be almost constant since about 1985. However, there are differences in the *UBV* systems in published data. The most homogeneous (and extensive) dataset are our *UBVRI* LCs obtained since February 1994. Unfortunately we have captured only a part of the spot cycle – increase and decrease in the brightness of Max II (a symmetric LC was observed in January 1999). Due to this fact, our combined LCs are slightly asymmetric. Hence, we have folded the data around phase 0.5. The resulting (direct plus folded) data were used to form normal points in 0.005 phase bins. The U passband observations displayed very large scatter due to the late spectral type of XY UMa and enhanced chromospheric activity. Therefore, we have excluded the U data from the orbital elements determination.

For the determination of the photometric elements we have used the synthetic LCs and the 1992 version (Wilson 1992) of the differential corrections code developed by Wilson & Devinney (1971) (W&D). Since the spectroscopic elements are reliably known, the *RV*s were not included in the optimization. We have fixed the mass ratio to $q = 0.61$ (Pojmanski, 1998). *BVRI* LCs were solved simultaneously. For each LC the values of σ were

Table 6. Published geometric parameters for XY UMa. Parameters not adjusted in the solution are denoted by superscript ^{a}. The standard errors of the elements are given in parentheses (see Table 2)

Source	method	Filters	r_1	r_2	i	q
Geyer (1980)	?	B	0.41	0.22	83.5	-
Jassur (1986)	Bu73	$BVRI$	0.35	0.24	77–78	0.67
Budding & Zeilik (1987)	BuZe87	$BVRI$	0.327(2)	0.168(2)	88.2(4)	0.73
Banks & Budding (1989)	BuZe87	$BVRI$	0.345	0.190	84	-
Arévalo & Lázaro (1990)	BuZe87	JK	0.325–0.341	0.164–0.172	88.2^a	-
Arévalo & Lázaro (1990)	BuZe87	JK	0.358	0.201	77.2^a	-
Lee (1993)	WD?	V	0.354(3)	0.199(1)	85.49(30)	0.530(34)
Hilditch & Bell (1994)	H79	$V(CCD)$	0.382(2)	0.215(2)	82.0(3)	0.60^a
Erdem & Güdür (1998)	WD92	B	0.360(2)	0.267(4)	76.10(30)	0.828(14)
Erdem & Güdür (1998)	WD92	V	0.355(5)	0.269(3)	75.66(36)	0.828(14)
Kjurkchieva et al. (2000)	Br	$BVRI$	0.350	0.207	80	0.6

Methods: Bu73 – Budding (1973), BuZe87 – Budding & Zeilik (1987), WD? – unspecified older version of Wilson & Devinney code, WD92 – Wilson & Devinney (1992), Br – Bradstreet (1993), H97 – Hill (1979)

evaluated as described by Wilson (1979). The initial parameters were taken from H&B. Mode 2 of the W&D code appropriate for the detached binaries was employed assuming synchronous rotation and zero eccentricity. For the computation of the monochromatic luminosities we have used the approximate atmospheric model option of the W&D program. Coefficients of the gravity darkening $g_1 = g_2 = 0.32$ (Lucy 1967) and $A_1 = A_2 = 0.5$ (e.g., Rucinski 1969) were fixed as appropriate for the convective envelopes. The limb darkening coefficients were interpolated from Table 1 of Al-Naimiy (1978). Although the presence of a third component in the system is highly probable, its contribution to the total light of the system is negligible in the visible region. Arévalo et al. (1994) ascribed a deformation on the high resolution $BVRI$ CCD images to the third component. They estimated the mean instrumental magnitudes of this component with respect to XY UMa, observed at the maximum to be $\Delta B = 5.45 \pm 0.09$ mag, $\Delta V = 5.05 \pm 0.08$ mag, $\Delta R = 4.38 \pm 0.01$ mag, $\Delta I = 3.62 \pm 0.01$ mag. The expected third light is therefore rather small – only 0.035 in the I passband. Hence we have fixed a zero third light in our analysis.

The effective temperature of the primary is not reliably known (see Sect. 7), hence we have performed several solutions for $T_{\rm eff} = 5200$, 5400, 5600 and 5800 K. Since the ratio of the depths of the minima is defined mainly by the ratio of the surface brightness of the components, the influence of the temperature of the primary component on the LC is rather small. Some information on the $T_{\rm eff}$ is conveyed through the limb darkening. We have performed separate solutions for each possible temperature of the primary component. The best χ^2 (0.030556) was obtained for $T_{\rm eff} = 5200$ K corresponding to the G9 – K0 spectral type. For 5800 K (G2) we got $\chi^2 = 0.032287$. The resulting photometric elements for the 5200 K solution are given in Table 7 and corresponding fits in Fig. 10. For this solution we have checked the published range of the orbital inclinations 77°–88° for the behaviour of χ^2. We have obtained reasonable fits only in the range 78°–83°,

Table 7. Photometric elements and their standard errors (σ) – i – inclination; $q = m_2/m_1$ – mass ratio; Ω_1, Ω_2 – surface potentials; r_1, r_2 – volume mean fractional radii; T_1, T_2 – polar temperatures. $\sum w(\mathrm{O–C})^2$ is the weighted sum of squares of residuals for all light curves. Parameters not adjusted in the solution are denoted by a superscript "a"

Element			σ
i [°]		80.86	0.14
q		0.61^a	–
Ω_1		3.3755	0.0043
Ω_2		4.2437	0.0143
r_1		0.3721	0.0006
r_2		0.2015	0.0010
T_1 [K]		5200^a	–
T_2 [K]		4125	7
	B	0.9442	0.00006
	V	0.9334	0.00008
$L_1/(L_1+L_2)$	R	0.9175	0.00010
	I	0.9007	0.00013
M_1^{bol} [mag]		4.93	–
M_2^{bol} [mag]		7.27	–
log g_1 [cm s^{-2}]		4.35	–
log g_2 [cm s^{-2}]		4.67	–
$\sum w(\mathrm{O–C})^2$		0.030556	–

where χ^2 varied about 5%. The minimum was reached for $i = 80.9°$. This value and corresponding mean fractional radii $r_1 = 0.372$ and $r_2 = 0.201$ are in close agreement to those obtained by H&B.

It is remarkable that the optimum geometric elements fit satisfactorily all LCs. The only departures from the fit occur in the B passband around the shoulders of the secondary minimum and in the I passband in the descending shoulder to the primary minimum. The optimum temperatures of the components give a rather later spectral classification, G9-K0V + K7V, than widely accepted in previous papers.

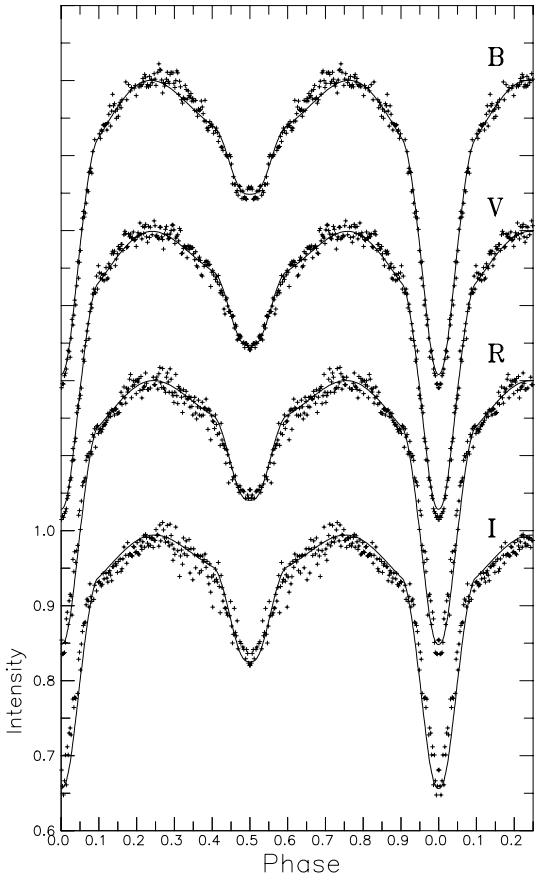

Fig. 10. *BVRI* normal points and best fits for $T_{\rm eff} = 5200$ K

7. Analysis of the individual light curves

The best photometric elements obtained from our LCs were used as the clean parameters for the star-spot modeling.

There are two widespread approaches to the spot modeling: (i) assumption of discrete circular starspots (ii) eclipse mapping using the maximum entropy method (MEM). The latter method requires data of excellent quality (Collier Cameron & Hilditch 1997). The first approach can provide rather reliable positions of one or two star spots. The results of the surface imaging by either of the methods depend much on the informational content and phase coverage of the data. The reliable determination of the spot temperatures requires multi-wavelength observations. Ordinary photoelectric photometry does not allow one to determine positions of the spots reliably. The most unsure parameter is the spot latitude (see e.g., Eker 1999), which correlates with its diameter. The reliability of the spot parameters depend on their position on the star. Parts of the stellar surface covered during the primary eclipse (in the case of XY UMa) can be imaged most reliably.

The published photometric observations of XY UMa vary in quality, phase coverage and number of observed passbands. Many observations were performed only in the V passband (see Table 8) and very often given only in the instrumental system. Therefore, we decided to analyze only our multi-wavelength observations using the circular-spots model. Our approach is close to the maximum probability method applied by Kürster & Schmitt (1999). We have found the maximally probable position of the first spot. If the χ^2 of the resulting fits was more than 10% higher than the χ^2 of the original data, we added another spot and so on. All observed LCs were explained sufficiently by one or two spots. The spots were assumed to be positioned only on the primary component since its contribution to the total light is more than 93% in the V passband.

The ratio of the spot and photosphere temperature (temperature factor) is highly correlated to the spot radius. Since there is only scanty information on latitudes of the spots that are not being eclipsed, we have fixed their latitudes to 0° (position of the equator). The resulting positions of the spots determined from our LCs are given in Table 9. The uncertainties in the spot latitudes is about 5°, while longitudes are unsure to about 1°. Resulting spot fits of all our LCs are displayed in Fig. 11. Our LCs have rather good time resolution. Hence we have identified the same spots on the subsequent LCs (see Fig. 12).

The spot fits fully explain the observations in the V, R and I passbands. The U and B LCs often show sudden increases in brightness, which cannot be explained by the presence of a hot spot, due to its short persistence. Such phenomena are well visible around the Max II on LCs 7 and 16. A small increase of the brightness is also visible on LCs 11 and 13 around Max I. The brightness increase reaches to about 7% of the total luminosity of XY UMa in the U passband, which substantially exceeds the strongest solar flares.

8. Absolute parameters of the system

The absolute parameters of the eclipsing pair were determined using the spectroscopic elements of Pojmanski (1998)(see Sect. 1) and inclination angle $i = 80.9°$ (see Table 7). The masses of the components are $m_1 = 1.10\ M_\odot$ and $m_2 = 0.66\ M_\odot$, Using the mean fractional radii of the components and the semi-major axis $a = 3.107 \pm 0.060\ R_\odot$, one can easily derive the absolute radii of the components: $R_1 = 1.16 \pm 0.02\ R_\odot$ and $R_2 = 0.63 \pm 0.01\ R_\odot$. The primary and secondary component fills 68% and 22% of their Roche lobes, respectively.

The distance determined indirectly from the absolute parameters is affected by three crucial parameters: the apparent visual magnitude of the system, the mean effective temperatures of the components and the interstellar extinction. The apparent visual magnitude $V = 9.5$ was determined from our observations. The effective temperatures of the components depend substantially on a spectral type – $T_{\rm eff}$ calibration and cannot be reliably determined from the LC modeling. The calibration of the bolometric correction, colours and effective temperatures on spectral types for the main sequence stars can be derived either from the observations of the Sun (Allen 1976) or UBV measurements of the standard stars

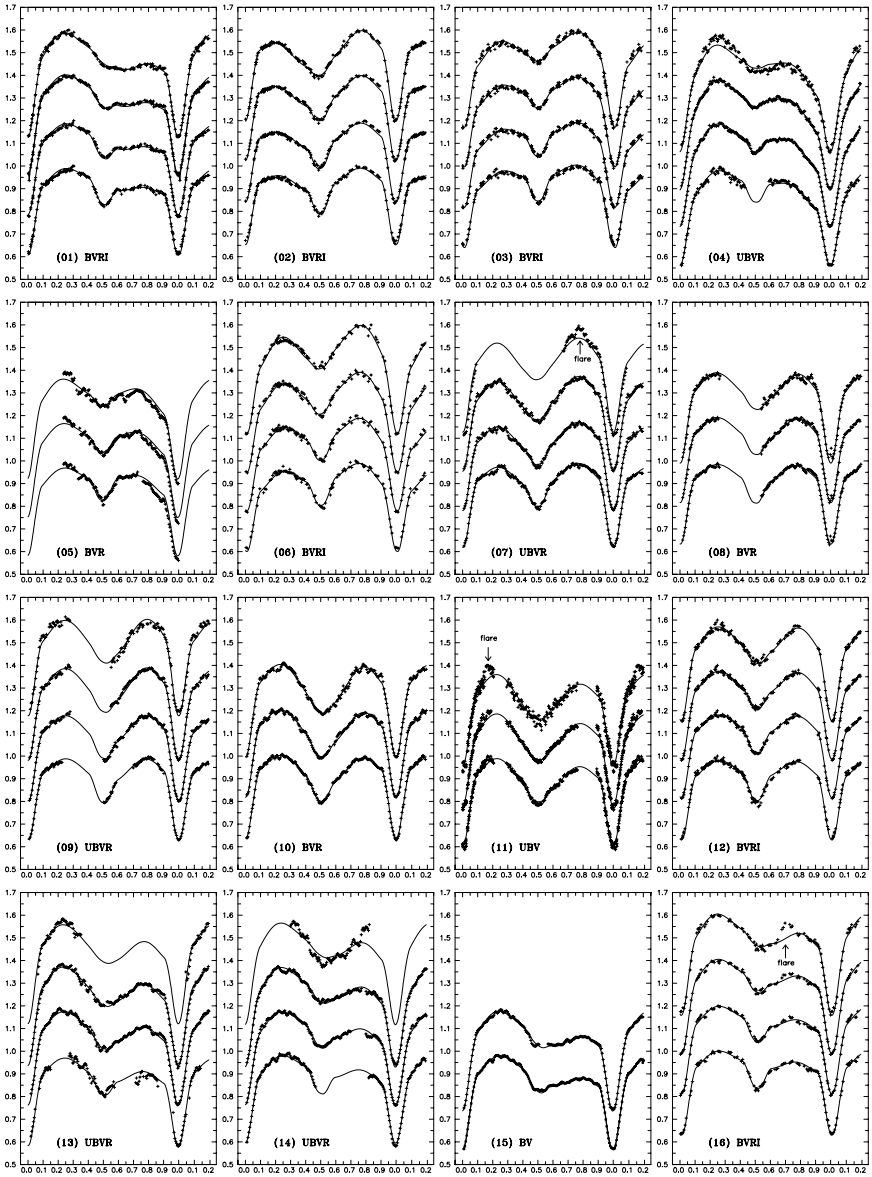

Fig. 11. Individual *UBVRI* light curves and their best spots fits corresponding to Table 9

(Popper 1980). The second calibration was accepted in our study. Since XY UMa is rather distant from the galactic plane ($b = +45.9°$), the interstellar extinction can be neglected.

The observed $(B-V)$ index of XY UMa in the maximum brightness is 0.77 mag. If we suppose that the observed light is reddened by the circumstellar absorption, the effective temperature of the primary can be 5400 K ($(B-V)_0 = 0.76$), 5600 K ($(B-V)_0 = 0.71$) or 5800 K ($(B-V)_0 = 0.66$), to get reasonable fit of the observed LCs. Visual absorption depends on the $(B-V)$ colour excess in such a way that for all three possible solutions we get the distance $d = 86 \pm 5$ pc, which is rather more than the Hipparcos distance 66 ± 6 pc. To get an accord with this value, the radius of the primary component would have to be reduced to about 0.85 $R_\odot$. For such a small radius of the primary, it is impossible to get a reasonable fit of the observed LCs. Hence, we must admit that the Hipparcos distance to XY UMa is not appropriate. The Hipparcos astrometry has been performed over only three years. The positions of XY UMa on the celestial sphere were affected by the presence of other component(s) of the system. To obtain reliable parallax, the astrometric observations should cover at least one orbital period of the 3rd body ($P_3 = 30$ years).

There are indications (LC solution, our estimate of the spectral type) that the spectral type of the primary component is rather later than the widely accepted G3V or G0V corresponding to its mass (Pojmanski 1998). In such a case, the radii and masses of the components are rather higher than expected for the main-sequence stars of the G9-K0+K7 spectral types. Pojmanski (1998) suggested that the primary component of XY UMa has already evolved (after some mass-transfer episode which might have caused significant surface cooling).

Table 9. Positions of the spots on the primary component. β – latitude, λ – longitude, R – radius and k – the temperature factor of the spot. The latitudes of the spots are measured from the equator. The longitudes are in the W&D notation i.e., a spot facing the observer during maximum I has longitude 270°, the longitudes can be simply transformed to the Binary Maker 2.0 notation by subtracting 360° – λ

LC	Filt.	β [°]	λ [°]	R [°]	k
01	*BVRI*	0[a]	113.2	30	0.919
		45	28.1	40	0.956
02	*BVRI*	0[a]	246.6	28	0.944
		0[a]	173.4	25	0.951
03	*BVRI*	−35	333.8	22	0.798
		0[a]	239.1	25	0.980
04	*UBVR*	0[a]	86.6	25	0.940
		19	14.2	30	0.903
05	*BVR*	48	39.4	35	0.912
06	*BVRI*	18	344.1	25	0.885
		0[a]	201.7	45	0.972
07	*UBVR*	0[a]	190.4	45	0.969
		40	334.4	25	0.964
08	*BVR*	0[a]	154.4	40	0.979
		−39	323.2	25	0.978
09	*UBVR*	0[a]	161.4	40	0.963
		34	320.3	20	0.954
10	*BVR*	0[a]	165.3	36	0.949
11	*UBV*	0[a]	176.9	40	0.957
		0[a]	68.7	25	0.958
12	*BVRI*	0[a]	159.5	35	0.974
		31	350.1	25	0.969
13	*UBVR*	0[a]	151.6	35	0.961
		43	47.4	25	0.906
14	*UBVR*	0[a]	126.7	38	0.965
		20	23.5	30	0.950
15	*BV*	0[a]	118.8	36	0.949
		30	25.5	33	0.961
16	*BVRI*	0[a]	114.9	35	0.960
		25	20.7	26	0.952

a – parameter not adjusted

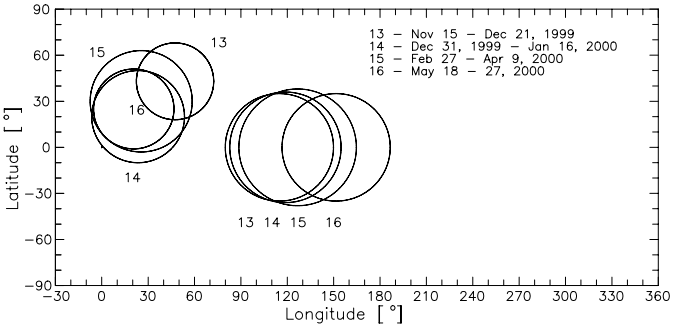

Fig. 12. Positions and diameters of the two spots identified in the 1999/2000 observing season

We must admit that the spectral classification of the system could be negatively influenced by an additional emissions decreasing the equivalent width of the hydrogen Balmer lines. Any attempt to analyze emisions in the Balmer lines without the knowledge of the true effective temperatures of the components is also questionable (e.g., Arévalo & Lázaro 1999). The temperature sensitive lines which are not affected by the emissions have to be used for the determination of the reliable spectral types of the components.

9. Conclusions

New *BVRI* photoelectric LCs obtained since 1994 allowed us to construct LCs without the maculation effect, suitable for the computation of the "clean" photometric elements. These data, together with published spectroscopic elements (Pojmanski 1998), yielded new absolute parameters of the eclipsing pair, i.e., masses $m_1 = 1.10\ M_\odot$, $m_2 = 0.66\ M_\odot$, radii $R_1 = 1.16\ R_\odot$, $R_2 = 0.63\ R_\odot$, luminosities $L_1 = 0.80\ L_\odot$, $L_2 = 0.093\ L_\odot$ (for $T_1 = 5200$ K), distance between the components $a = 3.107\ R_\odot$ and the inclination angle $i = 80.9°$.

One of the aims of our paper was to test the possible mechanisms of the long-term orbital period changes in XY UMa. We explained these changes by the presence of the third body in the system with an orbital period of 30 years. Its protostellar origin is supported by its observed infrared excess and the decrease of visual brightness of XY UMa during the inferior conjunction of this body in 1979. Long-term changes of the visual brightness of the system with a cycle at least 50 years does not support the possibility of explaining the 30 year orbital period variations by Applegate's mechanism. The differences in the maxima heights, which characterize the asymmetry of the LCs caused by the maculation effect, exhibit variations with a period of 709 ± 10 days. Nearly the same period (695 ± 17 days) has also been found in the (O–C) residuals from the third-body orbit. Hence the observed (O–C) diagram is the superposition of the LITE and maculation effects.

Our high-resolution spectroscopy of XY UMa revealed the changes in H_α profile due to emission, caused by the short-term enhanced chromospheric activity (flares) in XY UMa. We have occasionally detected flares also in our U and B LCs.

Although the new results improved our knowledge of XY UMa system, there are still some unsolved problems:

1) The $(B-V)$ colour index of the primary component, obtained during the eclipse of the secondary component, corresponds to the spectral type G8 – K1. If the primary component is on a main sequence, then it has to be underluminous for its spectral type, most probably due to the maculation effects. On the other hand, we have demonstrated that the maculation can also cause the change of the RV amplitudes, leading to erroneous masses of the components. To solve the problem definitively, it is necessary to fit the RV curve and photometric LCs taken simultaneously, most likely with the position of spots in quadratures.

2) The distance to XY UMa determined from absolute dimensions and luminosities of the components $d = 86 \pm 5$ pc is larger than the Hipparcos astrometric value

$d = 66 \pm 6$ pc. The discrepancy can be caused by the presence of a protostellar third body in the system, which affects the correct determination of the astrometric parallax of XY UMa, but can also be the source of the absorbing circumbinary matter, which influences the determination of the distance of XY UMa from luminosities.

Acknowledgements. This work was carried out during the stay of T. P. and D. C. in Naples. They would like to thank to CNR and OAC for support. P. A. H. would like to thank Ron Angione for scheduling the observing time at Mt. Laguna. The authors thank to Drs. Geyer, Scaltriti, Udalski, Pojmanski, Marchev, Hilditch and Collier Cameron for providing original photometric observations and discussion. This work has been supported by VEGA Grant 1157 (T. P., D. C. & S. P.), The Research Corporation, The American Astronomical Society Small Grants Program and Western Carolina University (P. A. H.).

References

Allen, C. W. 1976, Astrophysical Quantities (The Athlone Press, London)
Al-Naimiy, H. M. 1978, Ap&SS, 53, 181
Applegate, J. H. 1992, ApJ, 385, 621
Arévalo, M. J., & Lázaro, C. 1990, AJ, 99, 983
Arévalo, M. J., & Lázaro, C. 1999, AJ, 118, 1015
Arévalo, M. J., Lázaro, C., Martinez-Roger, C., et al. 1994, in Cool Stars, Stellar Systems and the Sun, ed. J. P. Caillault, ASP Conf. Ser., 64, 548
Baluta, C. J., Guinan, E. F., McCook, G. P., et al. BAAS, 23, 835
Banks, T., & Budding, E. 1989, Inf. Bull. Var. Stars No., 3304
Bedford, D. K., Jeffries, R. D., Geyer, E. H., et al. 1990, MNRAS, 243, 557
Bradstreet, D. H. 1993, Binary Maker 2.0, Dept. Phys. Science, Eastern College, St. Davids, PA, USA
Budding, E. 1973, Ap&SS, 22, 87
Budding, E., Kadouri, T. H., & Gimenez, A. 1982, Ap&SS, 88, 453
Budding, E., & Zeilik, M. 1987, ApJ, 319, 827
Chochol, D., Pribulla, T., Teodorani, M., et al. 1998, A&A, 340, 415 (C&P)
Collier Cameron, A., & Hilditch, R. W. 1997, MNRAS, 287, 567
Eker, Z. 1999, ApJ, 512, 386
Erdem, A., & Güdür, N. 1998, A&AS, 127, 257
Geyer, E. H., Kippenhahn, R., & Strohmeier, W. 1955, Kleine Veroff. Remeis Sternwarte Bamberg No., 9
Geyer, E. H. 1976, in Proc. IAU Symp. 73, Structure and Evolution of Close Binary Stars, ed. P. P. Eggleton, S. Milton, & J. Whelan (D. Reidel, Dordrecht), 313
Geyer, E. H., & Metz, K. 1977, Ap&SS, 52, 351
Geyer, E. H. 1977, Proc. IAU Coll. No., 42, 292
Geyer, E. H. 1980, in Close Binary Stars: Observations and Interpretation, ed. M. J. Plavec, D. M. Popper, & R. K. Ulrich (D. Reidel, Dordrecht), 423
Geyer, E. H., & Hoffmann, M. 1981, Mitt. Astron. Ges., 52, 70
Hanžl, D. 1991, Inf. Bull. Var. Stars No., 3615
Heckert, P., & Zeilik, M. 1988, Inf. Bull. Var. Stars No., 3253
Henden, A. A., & Kaitchuck, R. H. 1982, Astronomical Photometry (Van Nostrand Reinhold Company)
Henry, G. W., Eaton, J. A., Hamer, J., & Hall, D. S. 1995, ApJS, 97, 513
Hilditch, R. W., & Bell, S. A. 1994, MNRAS, 267, 1081 (H&B)
Hilditch, R. W., & Collier Cameron, A. 1995, MNRAS, 277, 747
Hill, G. 1979, Publ. Dom. Astrophys. Obs., 15, 297
Huisong, T., & Xuefu, L. 1987, A&A, 172, 74
Jassur, D. M. Z. 1986, Ap&SS, 128, 369
Jeffries, R. D., Collins, C., Elliott, K. H., et al. 1995, Inf. Bull. Var. Stars No., 4277
Jeffries, R. D. 1998, MNRAS, 295, 825
Kjurkchieva, D., Marchev, D., & Ogloza, W. 2000, A&A, 354, 909
Kreiner, J. M. 2000, private communication
Kürster, M., & Schmitt, J. H. M. M. 1992, in Surface Inhomogeneities on Late-Type Stars, Armagh bicentary Colloquium, ed. P. B. Byrne (Springer-Verlag, Berlin), 69
Kwee, K. K., & van Woerden, H. 1956, Bull. Astron. Inst. Nether., 12, 327
Landolt 1973, AJ, 78, 959
Landolt 1983, AJ, 88, 439
Lanza, A. F., & Rodonò, M. 1999, A&A, 349, 887
Lázaro, C., Arévalo, M. J. 1996, in Cool Stars, Stellar Systems, and the Sun, ed. R. Pallavicini, & A. Dupree, ASP Conf. Ser., 109, 651
Lee, W. B. 1985, Ph.D. Thesis, University of Bonn
Lee, W. B. 1993, in New Frontiers in Binary Star Research, ed. J. C. Leung, & I. S. Nha, ASP Conf. Ser. 38, 334
Li, Q., Zhang, X., & Zhang, R. 1989, Inf. Bull. Var. Stars No., 3374
Lorenzi, L., & Scaltriti, F. 1977, Acta Astron., 27, 273
Lucy, L. B. 1967, Z. Astrophys., 65, 89
Medeiros, J. R., & Mayor, M. 1999, A&AS, 139, 433
Pojmanski, G., & Geyer, E. H. 1990, Acta Astron., 40, 245 (P&G)
Pojmanski, G., & Udalski, A. 1997, Acta Astron., 47, 451
Pojmanski, G. 1998, Acta Astron., 48, 711
Popper, D. M. 1980, ARA&A, 18, 118
Pribulla, T., Chochol, D., & Parimucha, Š. 1999, Inf. Bull. Var. Stars No., 4751
Pribulla, T., Chochol, D., Rovithis-Livaniou, R., & Rovithis, P. 1999, A&A, 345, 137
Pribulla, T., Chochol, D., Milano, L., et al. 2000, A&A, 362, 169
Rainger, P. P., Hilditch, R. W., & Edwin, R. P. 1991, MNRAS, 248, 168
Rucinski, S. M. 1969, Acta Astron., 19, 245
Strassmeier, K. G., Hall, D. S., Fekel, F. C., & Scheck, M. 1993, A&AS, 100, 173
Wilson, R. E. 1979, ApJ, 234, 1054
Wilson, R. E. 1992, private communication
Wilson, R. E., & Devinney, E. J. 1971, Astrophys. J., 166, 605 (W&D)
Yeates, C. M., Hintz, E. G., Joner, M. D., et al. 2000, Inf. Bull. Var. Stars No., 4943
Zeilik, M., Batuski, D., Elston, R., et al. 1982, Inf. Bull. Var. Stars No., 2169
Zeilik, M., Elston, R., & Henson, G. 1983, AJ, 88, 532
Zeilik, M., Cox, D., De Blasi, C., et al. 1988a, Inf. Bull. Var. Stars No., 3200
Zeilik, M., De Blasi, C., Rhodes, M., et al. 1988b, ApJ, 332, 293
Zeilik, M., Cox, D., & De Blasi, C. 1989, ApJ, 345, 991
Zeilik, M., De Blasi, C., Gordon, S., et al. 1990, Inf. Bull. Var. Stars No., 3535